Theory of magnetism in diluted magnetic semiconductor nanocrystals

Shun-Jen Cheng
Department of Electrophysics, National Chiao Tung University, Hsinchu, Taiwan 30050, Republic of China
(Received 22 September 2007; published 10 March 2008)

We present a theoretical investigation of magnetism in II-VI diluted magnetic semiconductor nanocrystals (NCs). The energy spectra, magnetizations, and magnetic susceptibilities of singly charged NCs with few substitutional magnetic Mn^{2+} ions are studied as functions of NC size, magnetic dopant distribution, and concentration by using the technique of exact diagonalization. For NCs containing long range interacting Mn ions, the quantum size effects improve the stability of ferromagnetic magnetic polarons. The carrier-mediated spin interactions between magnetic ions result in the enhancement of magnetism. By contrast, the ground states of NCs containing short ranged Mn clusters undergo a series of magnetic phase transitions from antiferromagnetism to ferromagnetism, with decreasing size of NC. An analysis based on a simplified constant interaction model, supported by the numerical calculations of local mean field theory, is presented for the magnetic NCs with many magnetic ions over a wide range of Mn concentration and NC size. Accordingly, we derive the condition for the formation of magnetic polaron and predict the observable signatures of the magnetic phases in magnetization measurements.

DOI: 10.1103/PhysRevB.77.115310 PACS number(s): 75.75.+a, 75.30.Hx, 75.50.Pp

I. INTRODUCTION

Semiconductor quantum dots are known as promising building block in many advanced applications from optoelectronics, spintronics, to biotechnology.[1–4] Moreover, recent technical advances have made it possible to incorporate controlled number of magnetic ions, typically Mn^{2+}, into individual colloidal semiconductor nanocrystals[5–8] and self-assembled quantum dots.[9–13] Rich physical phenomena, such as giant Zeeman splitting,[14] magnetic polarons,[13,15,16] zero-field magnetization,[17–19] and rich fine structures of exciton-Mn complexes[9–12] in those magnetic nanostructures have been observed. The underlying physics of the most physical phenomena can be attributed to the intriguing spin interactions between magnetic ions and quantum confined carriers.

As compared with self-assembled quantum dots, nanocrystals (NCs) are particularly advantageous in size and shape control.[21] The sizes of NCs can be controlled over a wide range of diameters, typically from 1 to 10 nm, by delicate fabrication processes.[22] Significant size and shape effects on the electronic and optical properties of nanocrystals and nanorods have been identified in optical and resonant tunneling spectroscopies.[21,23–25] With the engineering of quantum confinement, it is possible to manipulate the carrier-Mn spin interaction effectively and further affect the effective magnetic couplings between Mn ions in magnetically doped NCs.[19,20,26] Such an effective control of magnetism is of importance in the development of functional nanodevices based on diluted magnetic semiconductors needed to fill the long existing gap between semiconductor technology and magnetoelectronics.[19,20,26–39]

In this work, we present a theory of magnetism in II-VI diluted magnetic semiconductor nanocrystals. The developed theory guides us to gain deep physical insight into the magnetism in diluted magnetic semiconductor (DMS) bulk and nanosystems and is helpful with developing the effective means of magnetism control. We focus on singly charged spherical NCs coupled to substitutional divalent magnetic ions Mn^{2+} via the *sp-d* interactions. We show that ferromagnetic magnetic polarons (MPs) are formed in charged NCs containing long range interacting Mn^{2+} and the size effects of NC improve the stability of MPs. By contrast, the NCs containing short ranged Mn clusters are found to exhibit various magnetic phases from antiferromagnetism (AF) to ferromagnetism (FM), tunable by means of size control and identifiable in temperature dependent magnetization measurements.

The paper is organized as follows. In Sec. II, we describe the model Hamiltonian for DMS NCs and the theoretical approaches for the calculation of the electronic and magnetic properties. In Sec. III, we present the numerical results for NCs with few (up to five) magnetic ions by using exact diagonalization and analyze the magnetic phase diagram of uniformly Mn-doped NCs with more magnetic ions within a simplified constant interaction model, in comparison with the numerical results calculated by the widely adopted mean field theory. We conclude in IV.

II. THEORY

A. Model

The Hamiltonian for a singly charged magnetic NC coupled to arbitrary number of magnetic ions can be expressed as[26,34,40]

$$H_0 = H_e + H_{\text{Mn-Mn}} + H_{e\text{-Mn}} + H_B. \quad (1)$$

Here, $H_e = \Sigma_{i\sigma} E_i c_{i\sigma}^{+} c_{i\sigma}$ is the single-electron Hamiltonian of Mn-free NC, where subscript i labels single-electron orbital states, $\sigma = \uparrow (\downarrow)$ denotes the up (down) spin of electron, $c_{i\sigma}^{+}$ ($c_{i\sigma}$) the creation (annihilation) operator, and E_i the eigenenergy of a single electron in state $|i\rangle$. We take the second quantized form of Eq. (1) here for straightforward implementation of exact diagonalization calculations based on configuration interaction theory.[34,36] Within the hard wall spherical

model,[36,41,42] the eigenstates of a single electron in a Mn-free symmetric NC are denoted as $|i;\sigma\rangle=|n,l,m;\sigma\rangle$, where n is the principal quantum number, l the angular momentum, m the z component of angular momentum, and the single-electron eigenenergies and wave functions are explicitly given by

$$E_{nlm}=\frac{\hbar^2\alpha_{nl}^2}{2m^*a^2} \tag{2}$$

and

$$\psi_{nlm}(\vec{r})=\langle\vec{r}|nlm\rangle=\sqrt{\frac{2}{a^3}}\frac{J_l\left(\frac{\alpha_{nl}}{a}r\right)}{J_{l+1}(\alpha_{nl})}Y_{lm}(\theta,\psi), \tag{3}$$

respectively, where $\vec{r}=(r,\theta,\phi)$ is the position of electron in polar coordinate, a the radius of spherical NC, m^* the effective mass of electron, $J_l(r)$ the spherical Bessel function, α_{nl} the nth zero of J_l, and $Y_{lm}(\theta,\psi)$ the spherical Harmonic function. Throughout this work, we take the values of the effective mass of electron $m^*=0.15m_0$ and the dielectric constant $\epsilon=8.9$ for CdSe NCs, with which we have the value of effective Bohr radius $a_B=3.1$ nm and that of the effective Rydberg Ry$^*=25.8$ meV.

The antiferromagnetic interaction between magnetic ions $H_{\text{Mn-Mn}}$ is short ranged and described by

$$H_{\text{Mn-Mn}}=-\frac{1}{2}\sum_{I\neq J}J_{MM}(R_{IJ})\vec{M}_I\cdot\vec{M}_J, \tag{4}$$

where $\vec{M}_I$ ($\vec{M}_J$) is the spin of the Ith (Jth) magnetic impurities Mn^{2+} at position $\vec{R}_I$ ($\vec{R}_J$) and $J_{MM}(R_{IJ})=J_{MM}^{(0)}\exp\{-\lambda[(R_{IJ}/a_0)-1]\}<0$ is the antiferromagnetic coupling constant, rapidly decreasing with increasing the distance between magnetic ions $R_{IJ}\equiv|\vec{R}_I-\vec{R}_J|$, where $J_{MM}^{(0)}=-0.5$ meV is the strength of the nearest-neighbor (NN) Mn-Mn interaction, $a_0=0.55$ nm is the lattice constant of NC material, and $\lambda=5.1$.[34] Here, we characterize a magnetic ion with its spin along and neglect the electrostatic potential effect since divalent Mn ions in II-VI compounds are isoelectronic with cations and neither introduce nor bind charged carriers.[26,33]

The contact ferromagnetic interaction between electrons and magnetic ions $H_{e\text{-Mn}}$ is expressed as

$$H_{e\text{-Mn}}=-\sum_{I,i,i'}\frac{J_{ii'}^{eM}(\vec{R}_I)}{2}[(c_{i'\uparrow}^+c_{i\uparrow}-c_{i'\downarrow}^+c_{i\downarrow})M_I^z+c_{i'\downarrow}^+c_{i\uparrow}M_I^+ + c_{i'\uparrow}^+c_{i\downarrow}M_I^-], \tag{5}$$

where the first term on the right-hand side (rhs) describes that the z components of electron spins act as an effective field acting on Mn spins M_I^z, and the last two terms involving operators $M_I^\pm\equiv M_I^x\pm iM_I^y$ cause electron spin flip scattering compensated by Mn spin flips. The strength of the e-Mn interaction is given by $J_{ii'}^{eM}(\vec{R}_I)\equiv J_{eM}^{(0)}\psi_i^*(\vec{R}_I)\psi_{i'}(\vec{R}_I)\propto a^{-3}$ determined by the coupling constant $J_{eM}^{(0)}=10.8$ meV nm$^3>0$ and the local carrier density at the positions where Mn ions are located.

$H_B=H_z+T_B$ denotes the terms introduced by the presence of magnetic field $\vec{B}\|\hat{z}$, i.e., the spin Zeeman term

$$H_z=-\sum_i(g_e\mu_BBs_i^z)c_{i\sigma}^+c_{i\sigma}-\sum_I(g_{\text{Mn}}\mu_BB)M_I^z \tag{6}$$

and the field induced kinetic energy term

$$T_B=\sum_{i\sigma}(\mu_B^*B)m_ic_{i\sigma}^+c_{i\sigma}+\sum_{ij\sigma}\mu_B^*\left(\frac{a}{2l_B}\right)^2BD_{ij}c_{i\sigma}^+c_{j\sigma}, \tag{7}$$

where $g_e=1.2$ ($g_{\text{Mn}}=2.0$) is the g factor of electron (Mn) in CdSe NCs, $\mu_B=e\hbar/2m_0[\mu_B^*=(m_0/m^*)\mu_B]$ the (effective) Bohr magneton, s_i^z the z component of electron spin, $l_B=\sqrt{\hbar/(eB)}$ the magnetic length, and D_{ij} defined as $D_{ij}\equiv\langle i|(x^2+y^2)/a^2|j\rangle$.[36] The first term on the rhs of Eq. (7) is referred to as the orbital Zeeman term and vanishes for a single electron with zero angular momentum ($m_i=0$) in the ground state (GS). The second term in Eq. (7) associated with Langevin diamagnetism is negligible for strongly quantized NCs subject to weak magnetic fields ($a\ll l_B$).[55–58] Thus, we have the magnetic field dependent Hamiltonian $H_B\approx H_z$. In other words, the magnetic response of a singly charged magnetic NC mainly involves the spin of electron. The contribution of electron orbital motion to the magnetization of system is negligible.

B. Numerical approaches

We employ the technique of exact diagonalization (ED) to calculate the energy spectra of single-electron-few-Mn complexes in magnetic NCs. We select a number N_s of lowest energy single-electron states and construct all possible electron-Mn configurations $|m_l,s_z;M_1^z,M_2^z,\ldots,M_N^z\rangle$ classified by the z component of the angular momentum of electron m_l, the z component of electron spin s_z, and the z component of the spin of the ith Mn ion $M_i^z=-5/2,-3/2,\ldots,5/2$. Then, we build up the corresponding Hamiltonian matrices and carry out direct diagonalization. The convergence of results is tested by increasing the number and choice of single-electron basis. For single-electron cases, converged results are obtained usually with only $N_s=2$ (with only the lowest electronic s orbital of NC) because of strong quantization energy of NCs (2 orders of magnitude larger than the electron-Mn interaction). The main numerical difficulty nevertheless comes from the fact that the total number of single-electron-many-Mn configurations $N_c\propto 6^{N_{\text{Mn}}}$ rapidly increases with increasing number of Mn. We employ the LANCZOS eigensolver to find the low-lying eigenstates and eigenenergies for large matrices with high accuracy.

The magnetization of magnetic NCs at temperature T is numerically calculated by evaluating the definition of magnetization,[43]

$$\mathbf{M}=-\left(\frac{\partial F}{\partial B}\right)_{T,V}=\frac{1}{\beta}\left(\frac{\partial\ln Z}{\partial B}\right)_T, \tag{8}$$

where $\beta=1/(k_BT)$, $Z=\Sigma_i\exp(-E_i\beta)$ is the canonical ensemble equilibrium partition function, E_i is the ith eigenen-

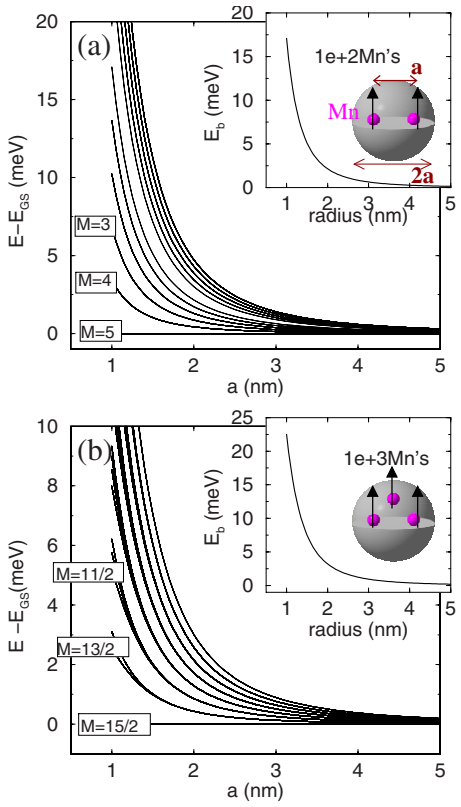

FIG. 1. (Color online) The energy spectrum relative to the GS energy of singly charged NCs with radius a doped with (a) two Mn ions positioned at $\vec{R}_1=(-a/2,0,0)$ and $\vec{R}_2=(a/2,0,0)$ and (b) three Mn ions at $\vec{R}_1=(-a/2,0,0)$, $\vec{R}_2=(a/2,0,0)$, and $\vec{R}_3=(0,0,a/2)$. The GSs of the NCs containing the long ranged Mn's are those of ferromagnetic MPs with maximum spin of Mn's. The insets show the binding energy E_b of the MPs versus NC radius. Note that E_b increases significantly as $a \lesssim a_B=3.1$ nm.

ergy of the system, and $F \equiv -\ln Z/\beta$ is the Helmholtz free energy. The magnetic susceptibility defined as the partial derivative of magnetization with respect to magnetic field, $\chi \equiv \partial \mathbf{M}/\partial B$, is calculated by the standard three-point numerical derivation.

III. NUMERICAL RESULTS AND ANALYSIS

A. Nanocrystals with few magnetic ions

We start with NCs doped with few magnetic ions, for which exact diagonalization studies are possible. Figure 1(a) shows the numerically calculated low-lying energy spectra (relative to the GS energy) of singly charged NCs doped with two Mn^{2+} ions at $\vec{R}_1=(X_1,Y_1,Z_1)=(a/2,0,0)$ and $\vec{R}_2=(X_2,Y_2,Z_2)=(-a/2,0,0)$. With the long spatial separation between Mn's $a(\gg a_0)$, we have $J_{MM} \to 0$ and the effective magnetic coupling between Mn's is dominated by the e-Mn interaction. The contact FM e-Mn interactions give rise to the magnetic ordering of Mn's, forming ferromagnetic MPs with the maximum spin of Mn's ($M_{GS}=5N_{\mathrm{Mn}}/2=5$). The insets of Fig. 1 show the calculated binding energy of the MPs, defined by $E_b \equiv E_{GS}(J_{eM} \to 0) - E_{GS}$ as a function of NC radius, where E_{GS} is the ground state energy of system and $E_{GS}(J_{eM} \to 0)$ is the energy of the lowest states calculated with disabling the e-Mn coupling. The binding energies of the MPs are positive for all NC sizes under consideration and increases monotonically with decreasing size of NC. Notable is the fact that the increase of E_b is particularly pronounced as $a \lesssim a_B=3.1$ nm. Similar features of magnetism are obtained also for NCs doped with three Mn^{2+} ions at $\vec{R}_1=(a/2,0,0)$, $\vec{R}_2=(-a/2,0,0)$, and $R_2=(0,0,a/2)$, as shown in Fig. 1(b).

To gain more physical insight, we carry out the following analysis based on a simplified constant interaction model extended from the theory by Gould *et al.*[17] In the simplified model, we consider a single electron frozen in the lowest s orbital and assume constant Mn-Mn and e-Mn interactions. Thus, we have the solvable effective spin Hamiltonian for a single-electron-many-Mn complex in magnetic NCs,

$$H_{eff} = -J_c \vec{s} \cdot \vec{M} - \frac{J_M}{2} \sum_{I \neq J} \vec{M}_I \cdot \vec{M}_J, \tag{9}$$

where $\vec{M}=\Sigma_I \vec{M}_I$ denotes the total spin of Mn's and $J_c \geqslant 0$ ($J_M \leqslant 0$) is the effective e-Mn (Mn-Mn) interaction constant. For uniformly Mn-doped NCs, we take $J_c \approx J_{eM}^{(0)}/(\frac{4}{3}\pi a^3)$ and $J_M \approx J_{MM}^{(0)} \exp\{-\lambda[(n_c x_{\mathrm{Mn}})^{-1/3}-1]\}$, where x_{Mn} is the Mn concentration and $n_c=4$ is the number of cation in a unit cell. With Eq. (9), we can choose J ($\vec{J} \equiv \vec{M}+\vec{s}$) and M as quantum numbers for labeling single MP states as $|J,M\rangle$ with $J=M \pm 1/2$. The eigenenergies of states $|J=M \pm 1/2, M\rangle$ are thus explicitly given by $E(M \pm \frac{1}{2}, M) = \mp \frac{J_c}{2} M + \frac{J_M}{2}[M(M+1) - 35N_{\mathrm{Mn}}/4]$, where $M=0,1,\ldots,5N_{\mathrm{Mn}}/2$ ($M=1/2, 3/2, \ldots, 5N_{\mathrm{Mn}}/2$) for even (odd) N_{Mn}. After some algebra, we derive the total spin of Mn's in the GS,

$$M_{GS} = \text{integer part}[|J_c/(2J_M)| + c] - c, \tag{10}$$

with the upper limit $M_{GS} \leqslant 5N_{\mathrm{Mn}}/2$, where $c=0$ (1/2) for even (odd) number of Mn's. Accordingly, we have the condition $|J_c/J_M| \geqslant 5N_{\mathrm{Mn}}$ for the formation of FM MP and that $|J_c/J_M| < 2$ under which electron-Mn complexes in NCs retain AF. The binding energy of MP with $M_{GS}=5N_{\mathrm{Mn}}/2$ reads

$$E_b = \frac{J_c}{2} M_{GS} - \frac{J_M}{2} M_{GS}(M_{GS}+1). \tag{11}$$

In dilute-Mn cases ($x_{\mathrm{Mn}} \to 0$), we have $J_M \to 0$ and $M_{GS}=5N_{\mathrm{Mn}}/2$, and the binding energy of MP is given by

$$E_b = \left(\frac{3}{8\pi}\right) \frac{M_{GS} J_{eM}^{(0)}}{a^3}, \tag{12}$$

determined by the strength of e-Mn interaction, the total spin of Mn's, and the size of NC. With the parameters for CdSe:Mn NCs used in this work, the binding energy of MP is estimated as $E_b \sim N_{\mathrm{Mn}}(a_B/a)^3 \times 10^{-1}$ meV. This accounts for the significant increase of E_b as $a \lesssim a_B$ shown in the insets of Fig. 1.

Figure 2(a) shows the calculated low-field magnetic susceptibilities $\chi(B/T \to 0) \equiv \chi_0$ (black solid line) of the

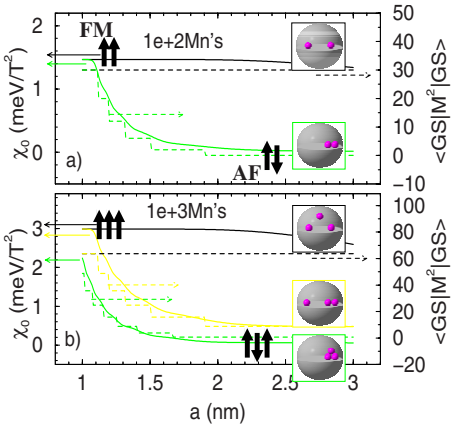

FIG. 2. (Color online) Size effects on the magnetic properties of magnetically doped NCs. The results are calculated by using exact diagonalization. (a) The low-field magnetic susceptibility $\chi_0 \equiv \chi(B/T \to 0)$ (solid lines) and the expectation values of M^2 for the ground states, $\langle \mathrm{GS}|M^2|\mathrm{GS}\rangle$ (dashed lines), as functions of NC radius a of singly charged NC coupled to two Mn's. Black [green (dark gray)] lines describe the results for the NC with long (short) ranged Mn's positioned at $\vec{R}_1=(-a/2,0,0)$ and $\vec{R}_2=(a/2,0,0)$ [$\vec{R}_1 \sim \vec{R}_2=(a/2,0,0)$]. (b) same as (a) but for NCs with three Mn's. The black, yellow (light gray), and green (dark gray) lines describe the results for the NCs with three different Mn distributions, i.e., $\{\vec{R}_1=(-a/2,0,0),\vec{R}_2=(a/2,0,0),\vec{R}_3=(0,0,a/2)\}$, $\{\vec{R}_1=(-a/2,0,0),\vec{R}_2 \sim \vec{R}_3=(0,0,a/2)\}$ and $\{\vec{R}_1 \sim \vec{R}_2 \sim \vec{R}_3=(0,0,a/2)\}$, respectively.

two-Mn NC at temperature $k_BT=0.1$ meV and the expectation values of M^2 for the ground states, $\langle \mathrm{GS}|M^2|\mathrm{GS}\rangle$ (black dashed line). The NCs containing the long ranged Mn's exhibit paramagnetism ($\chi_0 > 0$) over all sizes of the NCs under consideration. The susceptibilities of the quantum confined magnetic polarons can be well described by

$$\chi_0 = \frac{g_J^2 \mu_B^2 J(J+1)}{3k_BT}\left[1 - \frac{2(2J+1)e^{-\Delta/k_BT}}{(J+1)(2J-1)}\right], \qquad (13)$$

which is derived from Curie's law (the first term) concerned with only the GS level of MP with angular momentum $J=5N_{\mathrm{Mn}}/2+1/2$ and corrected by the weak effect from the next excited level states with $J-1$ (the second term), where $\Delta > 0$ is the energy difference between the ground states and the excited level states and $g_J=(g_s+g_{\mathrm{Mn}})/2+(g_{\mathrm{Mn}}-g_s)\cdot\frac{M(M+1)-S(S+1)}{2J(J+1)}$ is the Landé g factor ($g_J \sim 2$ as $M \gg S=1/2$). The numerically calculated susceptibilities $\chi_0 \sim 1.6$ meV/T^2, as shown in Fig. 2(a), are in agreement with the values evaluated by Eq. (13). With Eq. (13), it is straightforward to account for the slight decrease of the susceptibilities (black lines in Fig. 2) of the MPs confined in larger NCs (with smaller Δ).

In reality, the spatial distribution of magnetic ions in NCs is likely random.[5] To address the issue, we study another extreme case of nonuniformly Mn-doped NCs, which contain two nearest NN Mn's at $R_1, R_2 \sim (a/2,0,0)$ with $|R_1 - R_2| = a_0$. In bulk systems, such short range interacting Mn

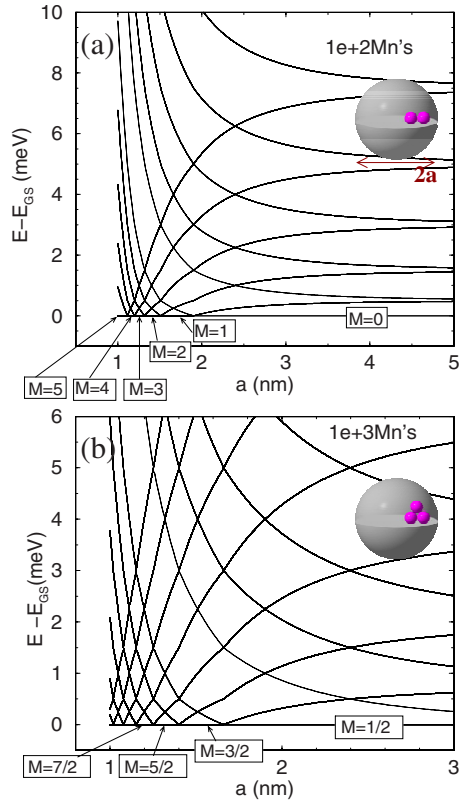

FIG. 3. (Color online) The energy spectrum relative to the GS energy of singly charged NCs with (a) two NN Mn's at $\vec{R}_1 \sim \vec{R}_2=(a/2,0,0)$ and (b) three NN Mn's at $\vec{R}_1 \sim \vec{R}_2 \sim \vec{R}_3=(a/2,0,0)$. The GSs of the NCs containing short ranged Mn clusters undergo a series of magnetic state transitions from antiferromagnetism ($M=0$) to ferromagnetism ($M=\frac{5}{2}N_{\mathrm{Mn}}$), with decreasing NC size.

clusters are known to exhibit AF and decrease the net magnetization of system.[33,44] Figure 3(a) shows the numerically calculated energy spectra of singly charged NCs containing the short ranged Mn's. In Fig. 2(a), we show the numerically calculated magnetic susceptibility (red solid line) and the total spin of Mn's (red dashed line) for the NC. For large NCs with $a > 1.9$ nm, the two-Mn cluster in the NCs exhibits AF ($M=0$) because the low electron local density at Mn sites leads to a weak electron-Mn coupling. With decreasing size of NC, the short ranged two-Mn cluster undergoes a series of magnetic state transitions from antiferromagnetism ($M=0$) to ferromagnetism ($M=5$). It turns to FM as the confinement of NC is so strong that the strength of the size-dependent e-Mn interaction is much larger than that of the AF Mn-Mn coupling. The magnetic susceptibility χ_0 of the NCs follows the same behavior as the total spin of Mn's, monotonically increasing with decreasing NC size.

The magnetic phases of magnetic MPs could be identified by carrying out the temperature dependent magnetization measurement.[19,20] Figure 4(a) shows the inverse of magnetic susceptibility χ_0^{-1} as a function of temperature for the NCs containing two NN Mn's with radii $a=1$, 2, and 3 nm, corresponding to the fully spin polarized (FM), partially spin polarized, and spin unpolarized (AF) GSs, respectively. For small NCs with $a \lesssim 1$ nm, χ_0^{-1} versus T follows Curie's law,

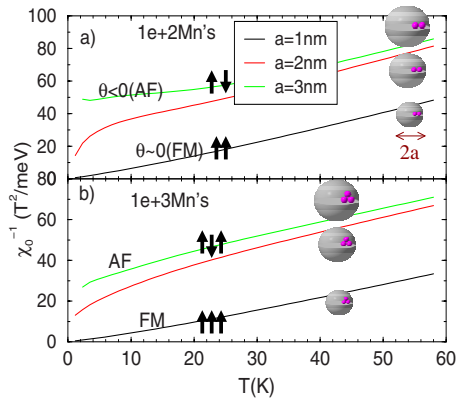

FIG. 4. (Color online) The reciprocal magnetic susceptibilities $1/\chi_0$ versus temperature (T) of magnetic NCs with various sizes ($a=1$, 2, and 3 nm) and containing (a) two short ranged NN Mn's at $\vec{R}_1,\vec{R}_2\sim(0,0,a/2)$ and (b) three NN Mn's at $\vec{R}_1,\vec{R}_2,\vec{R}_3\sim(0,0,a/2)$. The ground states of the NCs with the three different radii $a=1,2$, and 3 nm correspond to the fully spin polarized (FM), partial spin polarized, and spin unpolarized (AF) electron-Mn complexes, respectively. The reciprocal susceptibilities of the NCs with AF GSs follow the Curie–Weiss relation with negative Weiss temperature θ.

$\chi_0 \propto 1/T$, indicating the FM GSs. For large NCs with $a \gtrsim 3$ nm, the Mn clusters do not retain the magnetic ordering and the susceptibilities versus T follow the Curie–Weiss relation, $\chi_0 \propto 1/(T-\theta)$, with negative Weiss temperature $\theta<0$.[19,20]

Figure 2(b) shows the calculated magnetic susceptibilities and the total Mn spin of singly charged NCs containing three Mn's with different spatial distributions, as depicted in the figure. The temperature and quantum size dependences of the magnetic susceptibilities of the three-Mn NCs follow the similar behavior to that of the two-Mn NCs previously discussed.

B. Many-Mn magnetic polarons

For NCs containing more Mn's, it is nontrivial to solve the many-body problem because of the huge number of configuration basis required in numerical calculations. Nevertheless, the solvable model described by Eqs. (9)–(11) and (13) allows us to evaluate the total spin, the binding energies, and the magnetic susceptibility of charged NCs doped with many Mn's over a wide range of x_{Mn} and a. The validity of the simple model for NCs uniformly doped with few Mn ions is confirmed by exact diagonalization studies. For many-Mn NCs, we examine the validity and explore the limitation of the simplified model by means of the comparison with the numerical results of mean field theory.[26,37]

Figure 5 shows the χ_0 of singly charged NC with radius $a=3$ nm as a function of number of Mn ions calculated within the simplified model. In the regime of dilute-Mn concentration $N_{\mathrm{Mn}}<55$ ($x_{\mathrm{Mn}}<1.5\%$), the low-field susceptibility χ_0 increases monotonically with increasing number of Mn ions. In fact, the low-field magnetic susceptibilities of the NCs show a *quadratic* dependence on the number of Mn

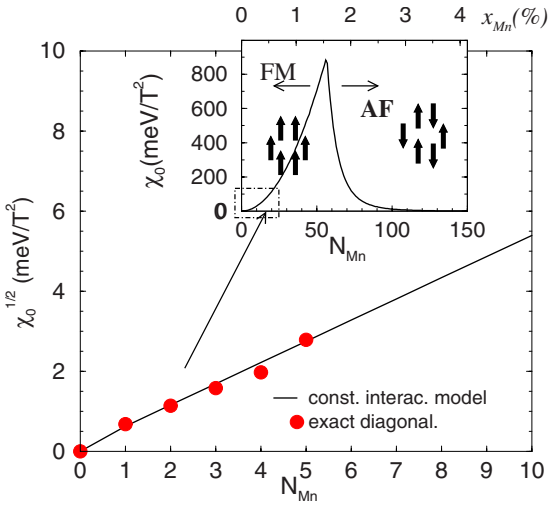

FIG. 5. (Color online) The low-field magnetic susceptibility χ_0 of magnetic polaron in a singly charged NC coupled to N_{Mn} Mn ions. The χ_0 calculated in the simplified constant interaction model (solid line) described by Eq. (9) shows quadratic dependence on small N_{Mn}, in agreement with the exact diagonalization results (red filled circles), indicating the formation of FM magnetic polarons in the regime. Inset: the χ_0 calculated within the simplified model over a wide range of N_{Mn}.

ions (see the inset of Fig. 5). Substituting the total spin $J=(5N_{\mathrm{Mn}}+1)/2$ of a FM MP into Eq. (13), we derive the χ_0 of magnetic NCs in the dilute-Mn regime,

$$\chi_0 \approx (25g_J^2\mu_B^2/12k_BT)N_{\mathrm{Mn}}^2. \tag{14}$$

If Mn ions were decoupled from each other, the total χ_0 would be simply the sum of magnetic susceptibility χ_{Mn} of each Mn ion, i.e., $\chi_0 \approx N_{\mathrm{Mn}}\chi_{\mathrm{Mn}}$, showing a linear dependence on N_{Mn}. The quadratic relationship indicates the existence of some spin correlation between Mn's, resulting in the enhancement of paramagnetism. The calculated χ_0 from the simplified model are in agreement with the results numerically calculated by ED for single MP in the NC with $N_{\mathrm{Mn}}=1,2,\ldots,5$ (see the inset of Fig. 5). In the ED calculation, we consider the NCs with the number of Mn ions up to 5, successively positioned at $R_1=(a/2,0,0)$, $R_2=(-a/2,0,0)$, $R_3=(0,0,a/2)$, $R_4=(0,0,-a/2)$, and $R_5=(0,0,0)$.

Figures 6 and 7 show the averaged Mn spin $\langle M\rangle \equiv M_{GS}/N_{\mathrm{Mn}}$ evaluated by Eq. (10) within the constant interaction model for NCs uniformly doped with many Mn ions, in comparison with the averaged Mn magnetization $\langle M\rangle_{MF}$ numerically calculated by the local mean field theory. Under the mean field treatment, the spatially discrete magnetic moments provided by magnetic Mn ions are replaced by an effective continuous field of Mn magnetization. The theory has been developed in various versions, widely applied to DMS bulks, thin films, and nanostructures. Here, we adopt the local mean field theory previously developed in Refs. 26 and 37 for magnetic quantum dots. A detailed description of the theory is given in the Appendix.

As we see in Figs. 6 and 7, the magnetizations of Mn-doped NCs as functions of Mn concentration and NC size

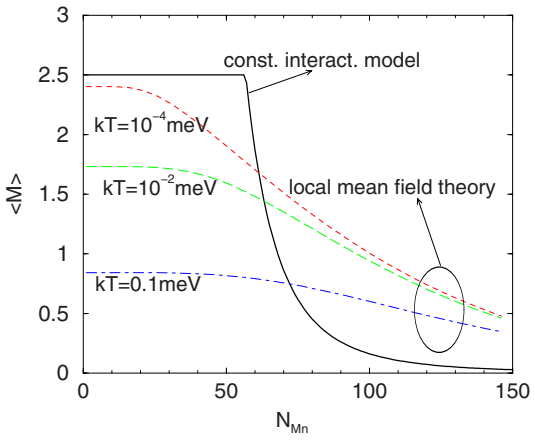

FIG. 6. (Color online) Averaged Mn spin of Mn-doped NC with radius $a=3$ nm as a function of Mn^{2+} number N_{Mn}. Black solid line: The averaged Mn spin $\langle M\rangle$ of the ground states calculated in the constant interaction model. Dashed lines: Averaged magnetization per Mn, $\langle M\rangle_{MF}$, calculated by local mean field theory for various temperatures.

predicted by both theories show similar basic features. For Mn-doped NCs with moderate Mn concentration ($N_{Mn} \lesssim 30$), averaged Mn magnetization is high (in nearly FM phases) and insensitive to the change of Mn number. The magnetization calculated by the mean field theory in the regime is generally lower than the averaged Mn spin calculated within the constant interaction model because of the effect of finite temperature. As $N_{Mn} \gtrsim 50$ ($x_{Mn} \gtrsim 1.5\%$), the Mn magnetization and the magnetic susceptibility as well (see the inset of Fig. 5) decrease rapidly with increasing N_{Mn}. In the regime, the Mn concentration is high so that the short ranged AF Mn-Mn interactions becomes comparable to the FM e-Mn interactions. However, the averaged Mn magnetization in the rich Mn regime seems to be underestimated in the constant interaction model because the exponentially decaying AF interaction between Mn's is assumed constant. Qualitatively, the results presented here are consistent with those previously reported by Fernandez-Rossier and Brey (Fig. 3 in Ref. 26).

Figures 7(a) and 7(b) show the magnetic phase diagram of Mn-doped NCs with respect to Mn concentration x_{Mn} and NC radius a calculated by using the constant interaction

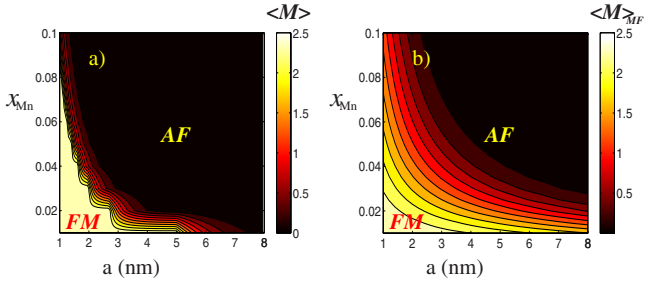

FIG. 7. (Color online) Averaged Mn spins of Mn-doped NCs as a function of Mn concentration x_{Mn} and NC radius a calculated within the constant interaction model (left panel) and by the local mean field theory for $T \to 0$ (right panel).

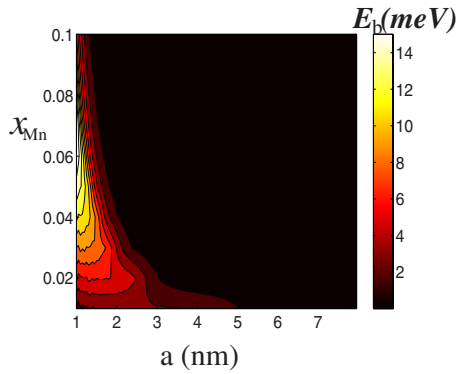

FIG. 8. (Color online) The binding energies, as a function of Mn concentration x_{Mn} and NC radius a, of magnetic polarons in Mn-doped NCs calculated within the constant interaction model.

model and the local mean field theory (for $T \to 0$), respectively. Both results show that NCs are in FM phase ($\langle M\rangle \to 5/2$) only if both Mn concentration x_{Mn} and NC size a are sufficiently small. The binding energies of the single-electron-many-Mn MPs as a function of Mn concentration x_{Mn} and NC radius a are evaluated by Eqs. (10) and (11) and shown in Fig. 8. Notable is the fact that the MPs confined in small Mn-doped NCs ($a < 2.5$ nm) possess the highest binding energy as the Mn concentration is moderately low $4\% < x_{Mn} < 8\%$ rather than extremely low. This is because the absolute value of E_b depends on both the spin polarization of Mn's and the number of Mn ions in NC [see Eq. (12) with $M_{GS} = \langle M\rangle \cdot N_{Mn}$]. Consequently, the most stable MPs are formed in small NCs but with the intermediately low Mn concentration.

IV. CONCLUSION

In summary, we present a theoretical investigation of magnetic properties of II-VI semiconductor nanocrystals incorporated with substitutional magnetic ions Mn^{2+}. For NCs with few magnetic ions, we carry out exact diagonalization for the calculation of the energy spectra, magnetizations, and magnetic susceptibilities of magnetic NCs with the number of Mn ions up to 5. For NCs with more Mn's, we take a simplified constant interaction model for the analysis of the electronic and magnetic properties of magnetic NCs over a wide range of NC size and Mn concentration. The issue of the validity of the simplified model for NCs with many Mn's is clarified by means of the comparison with the numerical results of mean field theory. We show that NCs containing short ranged Mn cluster can exhibit various distinctive magnetic phases from antiferromagnetism to ferromagnetism, tunable by means of the size control of NC. We derive the condition of magnetic polaron formation and predict the signatures of the magnetic phases observable in temperature dependent magnetization measurements as the manifestation of carrier-mediated magnetism in diluted magnetic semiconductors. The carrier-mediated spin correlation between magnetic ions results in the enhancement of paramagnetism evidenced by the quadratic relationship of magnetic susceptibility versus magnetic ion concentration.

ACKNOWLEDGMENTS

This work was supported by the National Science Council of Taiwan under Contract No. NSC-95-2112-M-009-033-MY3 and the National Center for High Performance Computing in Taiwan.

APPENDIX: LOCAL MEAN FIELD THEORY

In this appendix, we review the local mean field theory previously developed for diluted magnetic semiconductor nanostructures.[26,37] We employ the theory here for studying the magnetism of strongly quantized NCs uniformly doped with many Mn's, in comparison with the results given by the simplified constant interaction model.

In the spirit of mean field treatment, the e-Mn and Mn-Mn interactions in Eq. (1) are replaced by an Ising-like coupling between electron spin and a local effective field $h_{sd}(\vec{r})$ provided by the magnetization of Mn's. In the theory, the Hamiltonian of a singly charged NC with many Mn's is written as $H_\sigma^{MF}=H_e-s_z h_{sd}(\vec{r})$, where H_e is the single-electron Hamiltonian of Mn-free NC, the z component of electron spin is $s_z=\frac{1}{2}/-\frac{1}{2}$ for $\sigma=\uparrow/\downarrow$, and the local field h_{sd} experienced by the spin electron is given by

$$h_{sd}(\vec{r}) = J_{sd} n_{\mathrm{Mn}} \langle M_z(\vec{r})\rangle, \tag{A1}$$

where n_{Mn} denotes the density of Mn ions. The averaged local magnetization of Mn's reads

$$\langle M_z(\vec{r})\rangle = M B_M(Mb(\vec{r})/kT), \tag{A2}$$

where B_M is the Brillouin function and

$$b(\vec{r}) = \frac{J_{sd}}{2}(n_\uparrow - n_\downarrow) - J_{eff}^{AF}\langle M_z(\vec{r})\rangle \tag{A3}$$

is the local mean field felt by the Mn, $n_\sigma = \Sigma_i f(E_{i\sigma}^{MF};T)|\psi_\sigma^{MF}(\vec{r})|^2$ the mean value of electron density with spin σ, J_{eff}^{AF} is the effective field given by the AF interaction with neighbor Mn's, $f(E_{i\sigma};T) = \exp(-E_{i\sigma}/kT)/\Sigma_{j\sigma'}\exp(-E_{j\sigma'}/kT)$ is the occupancy probability of state $|i,\sigma\rangle$, and ψ_σ^{MF} is the single-electron wave function satisfying the Schrödinger equation

$$H_\sigma^{MF}\psi_\sigma^{MF} = E_\sigma^{MF}\psi_\sigma^{MF}. \tag{A4}$$

Since the AF Mn-Mn interaction spatially exponentially decays, here, we consider only the AF Mn-Mn interactions between the NN Mn's and take the form of the AF coupling $J_{eff}^{AF}=6J_{MM}^{(0)}\exp[-\lambda(\bar{d}/a_0-1)]$ in Eq. (A3), where $\bar{d}=n_{\mathrm{Mn}}^{-1/3}$ is the averaged distance between NN Mn's. Solving the coupled equations [Eqs. (A1)–(A4)], one can obtain the local field $b(\vec{r})$ and the averaged local magnetization per Mn ion $\langle M_z(\vec{r})\rangle$. The magnetism of a Mn-doped NC is characterized with the averaged Mn magnetization defined by $\langle M\rangle_{MF} \equiv \frac{1}{\Omega_{QD}}\int\langle M_z(\vec{r})\rangle d^3r$, where Ω_{QD} is the volume of NC.

For strongly quantized NCs at low temperatures, we can make some simplifications for the theory.[45–54] For magnetic NCs with high Mn concentration and finite magnetization (in the non-AF phase), electron spin is nearly fully polarized if the temperature $kT \ll \langle h_{sd}\rangle$. One can show that the condition is fulfilled as $kT \ll N_{\mathrm{Mn}} J_{sd}\Omega_{QD}^{-1}$. For the NCs considered in this work with typical volume $\Omega_{QD}\sim 10^2$ nm^3, the condition is satisfied as long as $N_{\mathrm{Mn}}>10$ and the thermal energy of temperature $kT \ll 1$ meV. Furthermore, for NCs with typical strong quantization $\sim 10^2$ meV ($\gg h_{sd}$), the influence of h_{sd} on the electronic structure of NC is negligible. Accordingly, we take the approximation $n_\uparrow - n_\downarrow \approx |\psi_\uparrow^{MF}|^2 \approx |\psi_\uparrow|^2$ in Eq. (A3), where $\psi=\sqrt{\pi/(2a^3)}\mathrm{sinc}(\pi r/a)$ is the wave function of the single-electron ground state of Mn-free NC in the hard wall sphere model and simplify Eq. (A3) to

$$b(\vec{r}) = \frac{J_{sd}}{2}|\psi(\vec{r})|^2 - J_{eff}^{AF} M B_M\,(Mb(\vec{r})/kT)\rangle. \tag{A5}$$

As a result, only Eqs. (A2) and (A5) are required to find the solutions of $b(\vec{r})$, $\langle M_z(\vec{r})\rangle$, and $\langle M\rangle_{MF}$. The numerically calculated $\langle M\rangle_{MF}$ by the local mean field theory for Mn-doped NCs with various sizes and Mn concentrations are shown in Figs. 6 and 7(b).

[1] D. D. Awschalom, D. Loss, and N. Samarth, *Nanoscience and Technology*, Semiconductor Spintronics and Quantum Computation Series (Springer-Verlag, Berlin, 2002).

[2] M. S. Skolnick and D. J. Mowbray, Physica E (Amsterdam) **21**, 155 (2004), and references therein.

[3] V. Cerletti, W. A. Coish, O. Gywat, and D. Loss, Nanotechnology **16**, R27 (2005), and references therein.

[4] W. J. Parak, D. Gerion, T. Pellegrino, D. Zanchet, C. Micheel, S. C. Williams, R. Boudreau, M. A. Le Gros, C. A. Larabell, and A. P. Alivisatos, Nanotechnology **14**, R15 (2003), and references therein.

[5] S. C. Erwin, L. Zu, M. I. Haftel, A. L. Efros, T. A. Kennedy, and D. J. Norris, Nature (London) **436**, 91 (2005), and references therein.

[6] F. V. Mikulec, M. Kuno, M. Bennati, D. A. Hall, R. G. Griffin, and M. G. Bawendi, J. Am. Chem. Soc. **122**, 2532 (2000).

[7] D. J. Norris, N. Yao, F. T. Charnock, and T. A. Kennedy, Nano Lett. **1**, 3 (2001).

[8] T. Ji, W. B. Jian, and J. Fang, J. Am. Chem. Soc. **125**, 8448 (2003).

[9] L. Besombes, Y. Leger, L. Maingault, D. Ferrand, H. Mariette, and J. Cibert, Phys. Rev. Lett. **93**, 207403 (2004); L. Besombes, Y. Leger, L. Maingault, D. Ferrand, H. Mariette, and J. Cibert, Phys. Rev. B **71**, 161307(R) (2005); Y. Leger, L. Besombes, J. Fernández-Rossier, L. Maingault, and H. Mariette, Phys. Rev. Lett. **97**, 107401 (2006).

[10] H. Mariette, L. Besombes, C. Bougerol, D. Ferrand, Y. Leger, L. Maingault, and J. Cibert, Phys. Status Solidi B **243**, 2709 (2006).

[11] J. Fernández-Rossier, Phys. Rev. B **73**, 045301 (2006).

[12] S. J. Cheng and P. Hawrylak, Europhys. Lett. **81**, 37005 (2008).
[13] P. Wojnar, J. Suffczyński, K. Kowalik, A. Golnik, G. Karczewski, and J. Kossut, Phys. Rev. B **75**, 155301 (2007).
[14] D. M. Hoffman, B. K. Meyer, A. I. Ekimov, I. A. Merkulov, Al. L. Efros, M. Rosen, G. Couino, T. Gacoin, and J. P. Boilot, Solid State Commun. **114**, 547 (2000).
[15] P. S. Dorozhkin, A. V. Chernenko, V. D. Kulakovskii, A. S. Brichkin, A. A. Maksimov, H. Schoemig, G. Bacher, A. Forchel, S. Lee, M. Dobrowolska, and J. K. Furdyna, Phys. Rev. B **68**, 195313 (2003).
[16] A. A. Maksimov, G. Bacher, A. McDonald, V. D. Kulakovskii, A. Forchel, C. R. Becker, G. Landwehr, and L. W. Molenkamp, Phys. Rev. B **62**, R7767 (2000).
[17] C. Gould, A. Slobodskyy, D. Supp, T. Slobodskyy, P. Grabs, P. Hawrylak, F. Qu, G. Schmidt, and L. W. Molenkamp, Phys. Rev. Lett. **97**, 017202 (2006).
[18] T. Gurung, S. Mackowski, H. E. Jackson, L. M. Smith, W. Heiss, J. Kossut, and G. Karczewski, J. Appl. Phys. **96**, 7407 (2004).
[19] I. Sarkar, M. K. Sanyal, S. Kar, S. Biswas, S. Banerjee, S. Chaudhuri, S. Takeyama, H. Mino, and F. Komori, Phys. Rev. B **75**, 224409 (2007).
[20] A. D. Lad, Ch. Rajesh, M. Khan, N. Ali, I. K. Gopalakrishnan, S. K. Kulshreshtha, and S. Mahamuni, J. Appl. Phys. **101**, 103906 (2007).
[21] D. Katz, T. Wizansky, O. Millo, E. Rothenberg, T. Mokari, and U. Banin, Phys. Rev. Lett. **89**, 086801 (2002); U. Banin, Y. Cao, D. Katz, and O. Millo, Nature (London) **400**, 542 (1999); U. Banin and O. Millo, Annu. Rev. Phys. Chem. **54**, 465 (2003).
[22] L. Brus, Appl. Phys. A: Solids Surf. **53**, 465 (1991).
[23] S. A. Empedocles, D. J. Norris, and M. G. Bawendi, Phys. Rev. Lett. **77**, 3873 (1996).
[24] N. Nirmal, B. O. Dabbousi, M. G. Bawendi, J. J. Macklin, J. K. Trautman, T. D. Harris, and L. E. Brus, Nature (London) **383**, 802 (1996).
[25] J. Hu, L. Li, W. Yang, L. Manna, L. Wang, and A. P. Alivisatos, Science **292**, 2060 (2001).
[26] J. Fernandez-Rossier and L. Brey, Phys. Rev. Lett. **93**, 117201 (2004).
[27] H. Ohno, D. Chiba, F. Matsukura, T. Omiya, E. Abe, T. Dietl, Y. Ohno, and K. Ohtani, Nature (London) **408**, 944 (2000); D. Chiba, M. Yamanouchi, F. Matsukura, and H. Ohno, Science **301**, 943 (2003).
[28] T. Jungwirth, J. Sinova, J. Masek, J. Kucera, and A. H. MacDonald, Rev. Mod. Phys. **78**, 809 (2006).
[29] J. I. Climente, M. Korkusinski, P. Hawrylak, and J. Planelles, Phys. Rev. B **71**, 125321 (2005).
[30] A. O. Govorov, Phys. Rev. B **70**, 035321 (2004); A. O. Govorov and A. V. Kalameitsev, *ibid.* **71**, 035338 (2005).
[31] A. K. Bhattacharjee and J. Perez-Conde, Phys. Rev. B **68**, 045303 (2003).
[32] J. K. Furdyna, J. Appl. Phys. **64**, R29 (1988).
[33] T. Dietl, Semicond. Sci. Technol. **17**, 377 (2002), and references therein.
[34] F. Qu and P. Hawrylak, Phys. Rev. Lett. **95**, 217206 (2005); F. Qu and P. Hawrylak, *ibid.* **96**, 157201 (2006).
[35] F. Qu and P. Vasilopoulos, Phys. Rev. B **74**, 245308 (2006).
[36] S. J. Cheng, Phys. Rev. B **72**, 235332 (2005).
[37] R. M. Abolfath, P. Hawrylak, and I. Zutić, Phys. Rev. Lett. **98**, 207203 (2007).
[38] K. Chang, S. S. Li, J. B. Xia, and F. M. Peeters, Phys. Rev. B **69**, 235203 (2004).
[39] Al. L. Efros, M. Rosen, and E. I. Rashba, Phys. Rev. Lett. **87**, 206601 (2001).
[40] I. Savic and N. Vukmirovic, Phys. Rev. B **76**, 245307 (2007).
[41] Y. Z. Hu, M. Lindberg, and S. W. Koch, Phys. Rev. B **42**, 1713 (1990).
[42] A. K. Bhattacharjee and C. Benoit a la Guillaume, Phys. Rev. B **55**, 10613 (1997).
[43] S. Blundell, *Magnetism in Condensed Matter* (Oxford University Press, New York, 2001).
[44] Q. Shen, H. Luo, and J. K. Furdyna, Phys. Rev. Lett. **75**, 2590 (1995).
[45] N. Q. Huong and J. L. Birman, Phys. Rev. B **69**, 085321 (2004).
[46] J. Seufert, G. Bacher, M. Scheibner, A. Forchel, S. Lee, M. Dobrowolska, and J. K. Furdyna, Phys. Rev. Lett. **88**, 027402 (2001).
[47] A. M. Yakunin, A. Yu. Silov, P. M. Koenraad, J. H. Wolter, W. Van Roy, J. De Boeck, J.-M. Tang, and M. E. Flatte, Phys. Rev. Lett. **92**, 216806 (2004).
[48] U. Banin, Y. Cao, D. Katz, and O. Millo, Nature (London) **400**, 542 (1999).
[49] D. L. Klein, R. Roth, A. K. L. Lim, A. Paul Alivisatos, and P. L. McEuen, Nature (London) **389**, 699 (1997).
[50] B. Alperson, S. Cohen, I. Rubinstein, and G. Hodes, Phys. Rev. B **52**, R17017 (1995).
[51] D. Klein, P. L. McEuen, J. E. Bowen Katari, and A. P. Alivisatos, Appl. Phys. Lett. **68**, 2574 (1996).
[52] E. P. A. M. Bakkers, Z. Hens, A. Zunger, A. Franceschetti, L. P. Kouwenhoven, L. Gurevich, and D. Vanmaekelbergh, Nano Lett. **1**, 551 (2001).
[53] M. Shim, C. Wang, and P. Guyot-Sionnest, J. Phys. Chem. **105**, 2369 (2001).
[54] P. Hawrylak, Phys. Rev. B **60**, 5597 (1999).
[55] S. J. Cheng, W. Sheng, and P. Hawrylak, Phys. Rev. B **68**, 235330 (2003).
[56] L. G. G. V. Dias da Silva and M. A. M. de Aguiar, Phys. Rev. B **66**, 165309 (2002).
[57] L. P. Levy, D. H. Reich, L. Pfeiffer, and K. West, Physica B **189**, 204 (1993).
[58] Y. Gefen, D. Braun, and G. Montambaux, Phys. Rev. Lett. **73**, 154 (1994).